

Application of Multiphoton Microscopic Imaging in Study of Gastric Cancer

Technology in Cancer Research & Treatment
Volume 21: 1-13
© The Author(s) 2022
Article reuse guidelines:
sagepub.com/journals-permissions
DOI: 10.1177/15330338221133244
journals.sagepub.com/home/tct



Xiaoying Wang, MD¹ , Di Zhang, MD², Xiaochun Zhang, MD, PhD³, Yuting Xing, BS⁴, Jihua Wu, MD¹, Xinke Sui, MD¹, Xin Huang, BD¹, Guoqing Chang, PhD⁴ , and Lianyong Li, MD, PhD¹ 

Abstract

Multiphoton microscopy (MPM) imaging relies on the nonlinear interaction between ultrashort optical pulses and the samples to achieve image contrast. Featuring larger penetration depth, less phototoxicity, 3-dimensional sectioning capability, no need for labeling, MPM become a powerful medical imaging technique that can identify structural characteristics of tissues at the cellular and subcellular levels. In this review paper, we introduce the working principle of MPM imaging, present the current results of MPM imaging applied to the study of gastric tumors, and discuss the future prospects of this interdisciplinary research field.

Keywords

multiphoton microscopy, 2-photon excited fluorescence, 3-photon excited fluorescence, second-harmonic generation, third-harmonic generation, gastric cancer

Abbreviations

AJCC, the American Joint Committee on Cancer; AUROC, the area under the receiver operating characteristic; CI, confidence interval; CG-E, chronic gastritis with erosion; CG-IM, chronic gastritis with intestinal metaplasia; EGC, early gastric cancer; EMR, endoscopic mucosal resection; ESD, endoscopic submucosal dissection; EUS, endoscopic ultrasonography; FAD, flavin adenine dinucleotide; H&E, hematoxylin-eosin; IM, intestinal metaplasia; ITA, intestinal-type adenocarcinoma; MPM, multiphoton microscopy; NADH, reduced form of nicotinamide-adenine dinucleotide; OPFE, 1-photon confocal fluorescence endoscopy; SHG, second-harmonic generation; THG, third-harmonic generation; ThPEF/3PEF, 3-photon excited fluorescence; TNM, tumor infiltration (T), lymph node metastasis (N) or distant metastasis (M); TPEF/2PEF, 2-photon excited fluorescence; SLAM, simultaneous label-free autofluorescence-multiphoton; SPM, self-phase modulation; UICC, the Union for International Cancer Control.

Introduction

Cancer is a leading cause of death worldwide and an important obstacle to prolonged lifespan.¹ The number of newly diagnosed gastric cancer worldwide exceeded 1 million in 2020, and the estimated death was 769,000 (ie, 1 of every 13 deaths is due to gastric cancer).² China has the highest incidence of gastric cancer in the world,³ which is second only to lung cancer, and the mortality rate ranks third⁴ with the age-standardized 5-year survival rate as low as 27.4%.³ The 5-year survival rate for gastric cancer exceeded 90% when diagnosed at an early stage, and dropped to only 10% to 20% at an advanced stage.^{5,6} With the rapid development of surgical techniques, traditional radiotherapy, neoadjuvant therapy, and endoscopic treatment in recent years, many scholars have

reported that the 5-year survival rate of patients with early gastric cancer (EGC) is approaching 95% or higher.^{7,8}

¹ Strategic Support Force Medical Center, Beijing, China

² Ningxia Jingyuan County People's Hospital, Ningxia, China

³ General Hospital of Ningxia Medical University, Ningxia, China

⁴ Institute of Physics, Chinese Academy of Sciences, Beijing, China

Corresponding Author:

Guoqing Chang, Key Laboratory of Optical Physics, Institute of Physics, Chinese Academy of Sciences, Beijing 100190, China.
Email: guoqing.chang@iphy.ac.cn

Lianyong Li, Department of Gastroenterology, Strategic Support Force Medical Center, 9 Anxiang Beili, Chaoyang District, Beijing 100101, China.
Email: Liliyong001@163.com



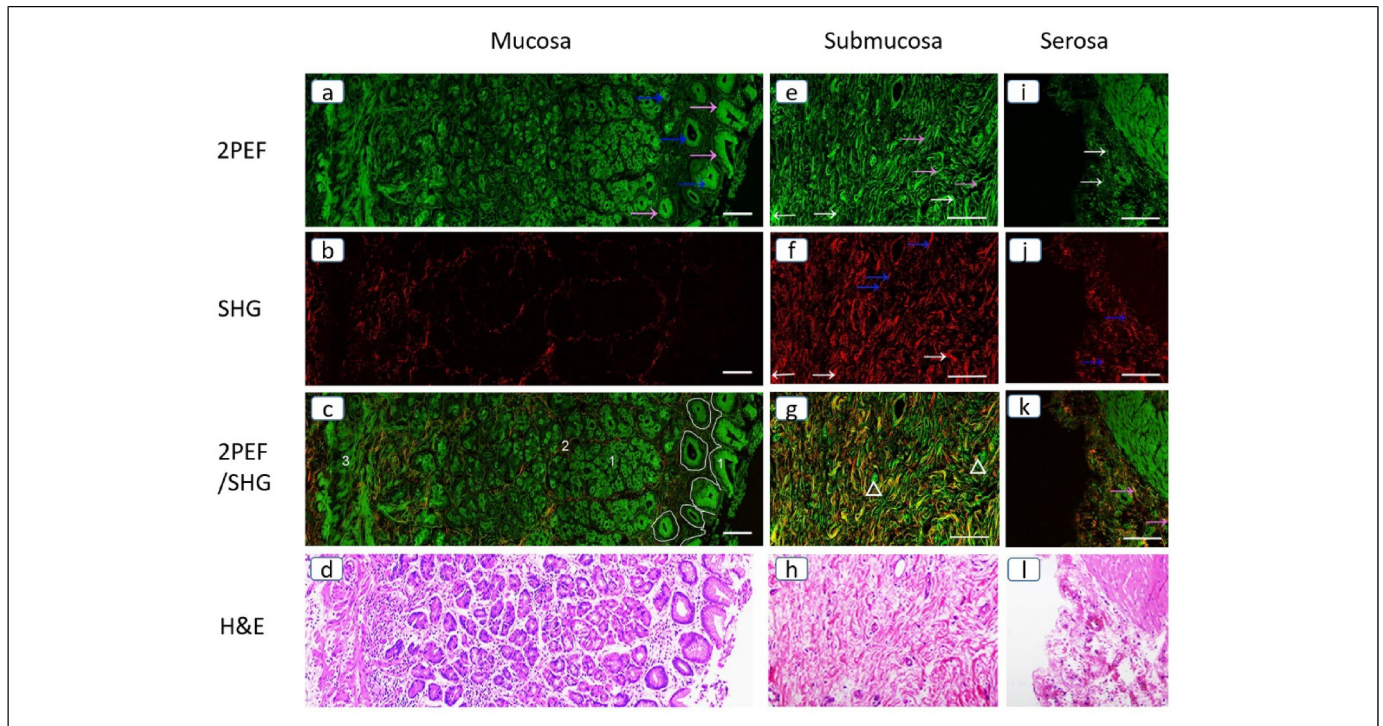


Figure 1. MPM images and corresponding H&E-stained images of normal gastric tissue.⁵⁵ Row 1: TPEF images (green), row 2: SHG images (red), row 3: overlaid TPEF/SHG images, row 4: corresponding H&E-stained images (20× magnification). Column 1: normal gastric mucosa. (a) TPEF image (blue arrows: fluorescent cytoplasm derived from NADH and FAD, pink arrows: nonfluorescent nuclear), (b) SHG image, (c) overlaid TPEF/SHG image (white curves: basement membrane, position1: epithelium and glands, position2: lamina propria, position3: muscularis mucosa), and (d) H&E-stained image. Column 2: normal gastric submucosa. € TPEF image (pink arrows: elastic fibers, white arrows: collagen bundles), (f) SHG image (blue arrows: collagen fibers, white arrows: collagen bundles), (g) overlaid TPEF/SHG image (triangle: blood vessels), (h) H&E-stained image. Column 3: normal gastric serosa. (i) TPEF image (white arrows: elastic fibers), (j) SHG image (blue arrows: collagen fibers), (k) overlaid TPEF/SHG (pink arrows: collagen bundles), (l) H&E-stained image. Scale bar: 100 μ m. These images are adapted from He et al [55]. MPM, multiphoton microscopy; TPEF, 2-photon excited fluorescence; SHG, second-harmonic generation; FAD, flavin adenine dinucleotide; H&E, hematoxylin-eosin; NADH, reduced form of nicotinamide-adenine dinucleotide

Histopathological diagnosis of gastrointestinal tumors by endoscopic biopsy is the gold standard. However, tissue biopsy has some drawbacks such as bleeding, perforation of digestive tract, small sampling tissue, inaccurate location, and time-consuming pathological sectioning process, which limit the timeliness and accuracy of endoscopic diagnosis of digestive tract tumors. Ideally, such highly invasive methods should be avoided especially for EGC diagnosis. Recent years have seen tremendous progress in development of multiphoton microscopy (MPM) aiming to conduct optical virtual biopsies. MPM relies on the nonlinear interactions between ultrashort optical pulses and the biomedical tissues—eg, second-harmonic generation (SHG), third-harmonic generation (THG), 2-photon excited fluorescence (TPEF), and 3-photon excited fluorescence (ThPEF)^{9–13}—to provide rich imaging contrast mechanisms. The generation of harmonic signals is an instantaneous coherent process^{14,15} and the most widely used at present is SHG, which originates from nonlinear interaction between light and noncentral symmetric structures. Consequently, SHG imaging can directly observe tissue structure with no need for labeling. As a third-order nonlinear optical process, THG signal arises from optical heterogeneity and can reveal lipid bodies, membranes,

cell outlines, elastin fibers etc.^{9,16,17} Compared with SHG microscope, no specific symmetry is required in the material to generate THG signal.¹⁸ Different from harmonic generation processes (eg, SHG, THG), multiphoton excited fluorescence involves absorption of multiple photons simultaneously by the molecules/atoms. Label-free imaging modalities of TPEF and ThPEF become possible thanks to the autofluorescence from various endogenous chromophores such as NAD(P)H, flavin adenine dinucleotide, collagen, elastin, tryptophan, etc These substances in living biological structures can have 2-photon/3-photon absorption in a wide wavelength range and emit broadband autofluorescence.¹⁹ Consequently, 2 different substances may have a large portion of spectral overlap for both absorption and emission, and thus careful attention should be paid to select the proper combination of the excitation and detection wavelength in order for a convincing differentiation.

MPM constitutes an enabling tool to achieve nondestructive, label-free imaging of biomedical tissues.^{16,20–23} Despite the lack of comparative study between MPM and single-photon imaging technologies for use in gastric cancer research, one of the main advantages of MPM imaging is its ability to provide optical sections with subcellular resolution and larger

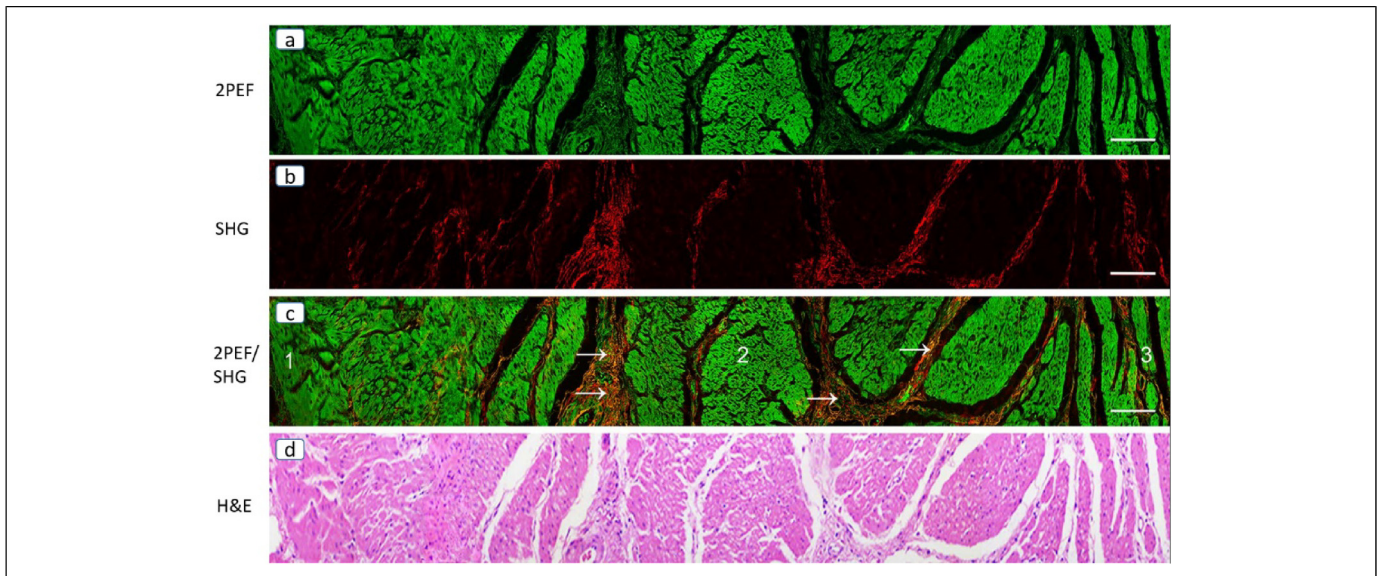


Figure 2. MPM images and H&E image of normal gastric muscle tissues.⁵⁵ (a) TPEF image, (b) SHG image, (c) overlaid TPEF/SHG image. Position 1-3 mark external longitudinal muscle, midterm circular muscle, and internal oblique muscle, respectively. White arrows: septa in the muscle tissues. (d) H&E-stained image (20× magnification). Scale bar: 100 μm .⁵⁵ Abbreviations: MPM, multiphoton microscopy; TPEF, 2-photon excited fluorescence; SHG, second-harmonic generation; H&E, hematoxylin-eosin

imaging depth in the scattered biological specimen.²⁴ Single-photon excited microscopy demands excitation light in the visible wavelength range, and the excitation pulses for MPM center at much longer wavelength in the infrared range. Although different tissues exhibit varied scattering properties,²⁵ longer excitation wavelength in general experiences less scattering loss and hence MPM features much larger imaging depth into the tissue.^{10,23} Ramos-Gomes applied both single-photon and 2-photon methods to imaging human micrometastatic and spreading tumor cells.²⁶ Their results demonstrated that the TPEF decayed much slower compared with single-photon confocal microscopy when imaging deeper into the tissue. Consequently, TPEF has a better signal-to-background ratio that results in an increased imaging depth.²⁶ Another advantage of MPM is that it provides imaging modalities (eg, SHG, THG) that are not available for single-photon-based methods.

MPM imaging offers several advantages over traditional pathohistology such as the capability of 3-dimensional imaging thanks to intrinsic optical sectioning, various label-free imaging contrast mechanisms, large penetration depth, and less phototoxicity.^{27,28} MPM has been widely used in the research fields of neurobiology, embryo development, tumor and so on,^{29–38} and here we review recent progress on applications of MPM imaging in the study of gastric tumors.

Application of MPM in Study of Gastric Tumors

Since its invention, MPM has found broad applications in tumor research such as tumor microenvironment monitoring,^{36,39–44} tumor metabolism,^{43,45–49} and tumor radiofrequency ablation

therapy.⁵⁰ Much progress has been made to apply MPM to study gastric cancers. Most of the current gastric cancer studies utilized the combination of 2-photon excited autofluorescence of autologous intrinsic fluorophores and SHG from collagen to provide detailed, real-time information on tissue structure and cellular structure morphology. Careful analysis of observed cell size and arrangement pattern, glandular morphology, collagen fiber alignments, collagen content, and inflammatory cell infiltration allows establishing MPM features associated with gastric tumors. Quantitatively measuring cell nuclear perimeter, nucleoplasmic ratio, nuclear area, collagen strength, and collagen fiber arrangement direction enables differentiation of normal tissues, diseased tissues, and tumor lesions. It is generally accepted that the occurrence and development of gastric cancer experience multiple steps: chronic superficial gastritis, atrophy, intestinal metaplasia (IM), dysplasia, and invasive cancer.⁵¹ IM and dysplasia are also called precancerous lesions of gastric cancer. IM is a pathological state in which gastric mucosal epithelial cells are replaced by intestinal epithelial cells. Correa⁵¹ suggested that IM might be the earliest indicator of potential malignant progression of gastric cancer. Early diagnosis and treatment can improve the prognosis of gastric cancer patients, but the proportion of EGC is only about 20% in China, and most gastric cancer cases are already in the advanced stage at diagnosis.⁴ Therefore, it is extremely important to screen precancerous lesions and EGC as early as possible. MPM offers real-time, label-free imaging at cellular and subcellular level, which makes it suitable for identifying EGC and monitoring tumor progression. In the following sections, we review the progress of utilizing MPM to image, identify, and investigate gastric cancers.

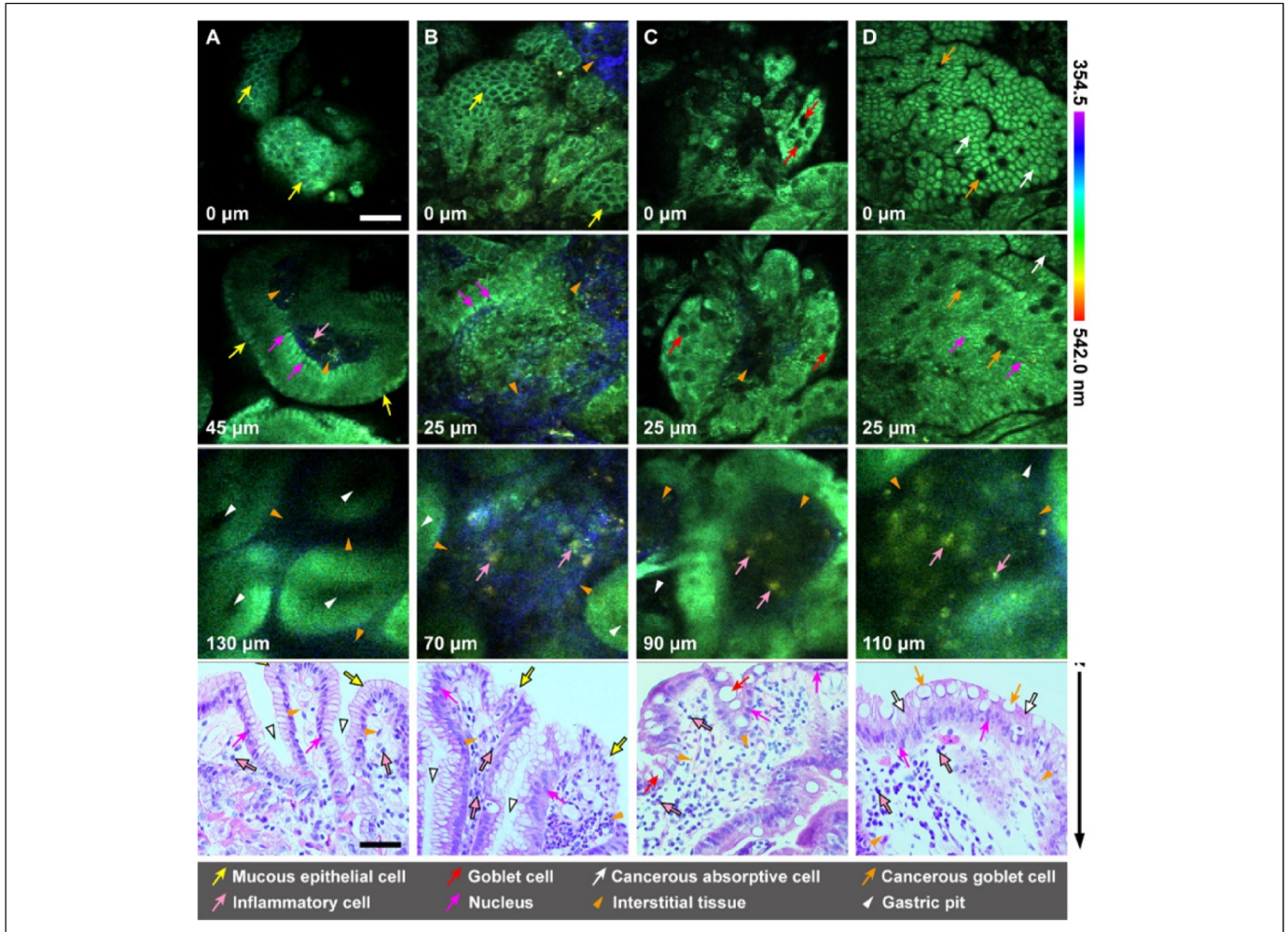


Figure 3. MPM images (first 3 rows, transverse view) and corresponding histology (last row, longitudinal view) of the normal and diseased human gastric antrum mucosa, the TPEF signal generated by NADH from the surface epithelium shown as green, and the SHG signal of collagen from the interstitial tissue of the lamina propria shown in blue. A column: normal, B column: chronic gastritis with erosion, C column: chronic gastritis with intestinal metaplasia, and D column: intestinal-type adenocarcinoma. The depth is labeled in the bottom left corner of each panel for TPEF images. Scale bar: 50 μm . This figure is adapted from Figure 4 in Li et al.⁴⁹ Abbreviations: MPM, multiphoton microscopy; TPEF, 2-photon excited fluorescence; SHG, second-harmonic generation; NADH, reduced form of nicotinamide-adenine inucleotide

MPM Imaging of Normal Gastric Tissue

Establishing diagnostic features by comparing lesioned gastric tissues with normal tissues is critical for early diagnosis of gastric cancer at the cellular level.⁵² The mucosal epithelial cells of normal gastric tissues are uniform in size and morphology; their nuclei also have similar size without stacking, and the size ratio between nucleus and cytoplasm falls in the range of 1:4 to 1:6. In contrast, most malignant tumors appear to have 3 main characteristics: differentiation and anaplasia, local infiltration, and metastasis.⁵³ Anaplasia refers to dedifferentiation, which is a credible indicator of malignancy, and anaplasia cells often exhibit the following morphological features: (1) pleomorphism (ie, cells exhibiting different sizes and morphologies), (2) nuclear abnormalities (deep-stained nuclei, varied size and shape, enlarged nuclei, and a nucleoplasmic ratio close to 1:1), (3) formation of tumor giant cells with 1 giant

nucleus or multiple nuclei, (4) untypical mitosis that may appear as tri- or quadri-polar mitotic images, and (5) loss of polarity and hence lack of recognizable orientation patterns among the anaplasia cells.⁵³ As the cancer grows, it is often accompanied by gradual infiltration, invasion, and destruction of adjacent tissues. Metastasis to a site which is discontinuous with the primary tumor is also a sign of malignancy.⁵³ As the first step, various research groups have adopted MPM to image normal gastric tissues in order to identify multiphoton diagnostic features. The stomach wall is divided into 4 layers: mucosa layer, submucosa layer, muscularis propria layer, and serosa layer. Current studies have demonstrated that a combination of TPEF and SHG can display the morphological characteristics of normal stomach and abnormal tissues. Rogart et al.²² found that columnar epithelial cells and gastric glands of gastric pits can be clearly imaged by MPM imaging of biopsy specimens of unstained digestive tract tissues. Especially the

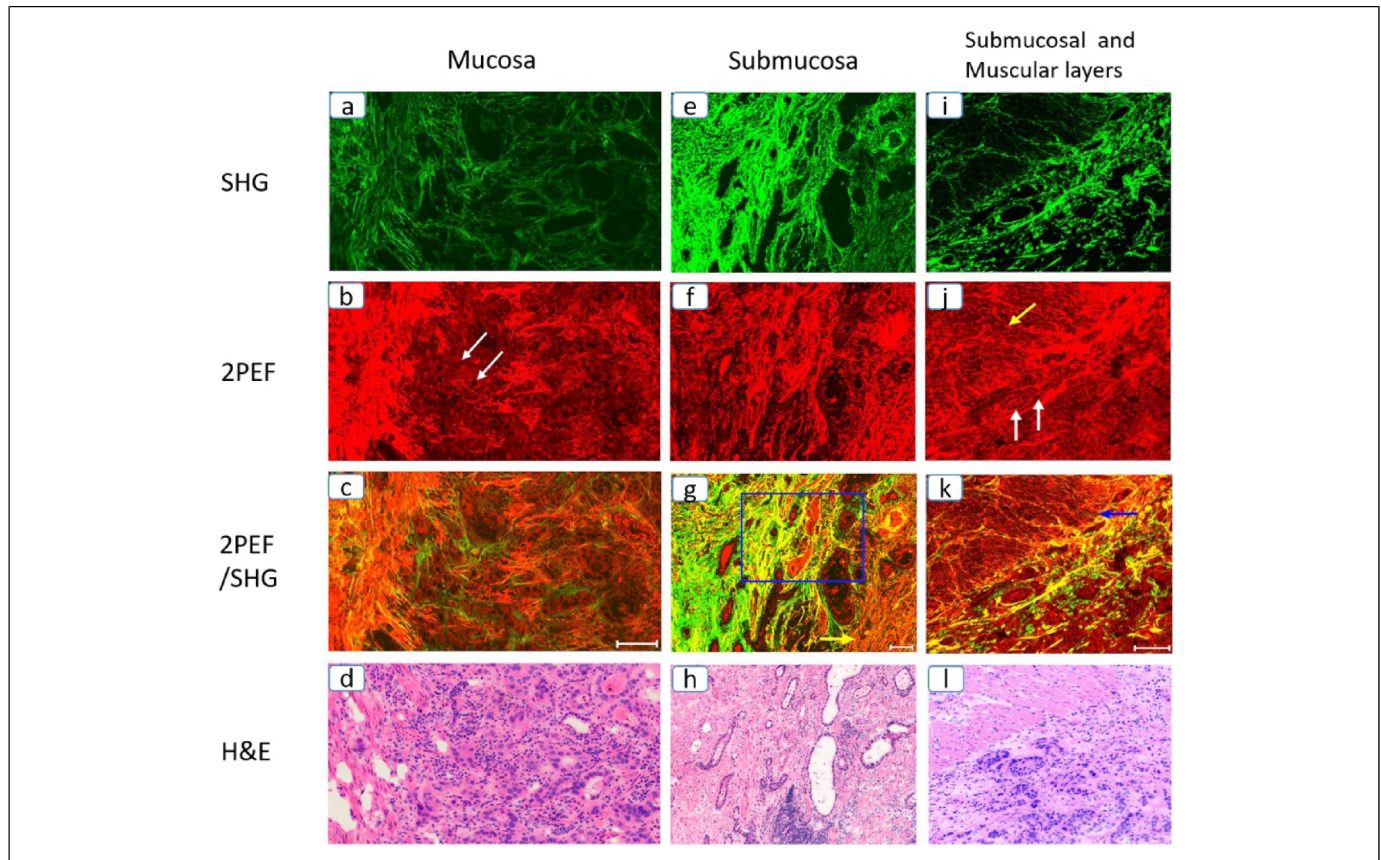


Figure 4. MPM images and H&E images of EGC.⁵⁸ Column 1: EGC invading the mucosa alone (a: SHG image, b: TPEF image, c: overlaid TPEF/SHG image, d: H&E-stained image), white arrow: cancerous cells. Column 2: EGC invading into submucosa (e: SHG image, f: TPEF image, g: overlaid TPEF/SHG image, h: H&E-stained image), Yellow arrow: muscularis mucosae. Column 3: boundary between submucosal and muscular layers in EGC (i: SHG image, j: TPEF image, k: overlaid TPEF/SHG image, l: H&E-stained image), Yellow arrow: elastic fiber, white arrow: malignant tumors, blue arrow: muscularis propria. Scale bar: 100 μm .⁵⁸ Abbreviations: EGC, early gastric cancer; MPM, multiphoton microscopy; TPEF, 2-photon excited fluorescence; ThPEF, 3-photon excited fluorescence; SHG, second-harmonic generation; H&E, hematoxylin-eosin.

connective tissue separating individual glands can be detected by SHG.²² The study shows that MPM can reveal the details of cell and subcellular structure in nonfixed and unstained gastrointestinal mucosa.²² Yan et al⁵⁴ also used MPM to image normal gastric tissue showing uniform epithelial cells, unchanged polarity with no nuclear overlap, and normal structures of gastric pits and gastric glands. The cell gap and nucleus morphology were also clearly visible, and individual glands were clearly identified.⁵⁴ Another study also confirmed that MPM imaging of normal gastric mucosa and submucosa clearly displayed the cell and subcellular structure of mucosa epithelium, lamina propria, and submucosa.⁵² In 2018, He et al⁵⁵ employed SHG and TPEF to image gastric mucosa, and submucosa (Figure 1a to h). The team also utilized these 2 imaging modalities (ie, SHG and TPEF) to show that the clear intrinsic muscle layer consists of internal oblique muscle, midterm circular muscle, and external longitudinal muscle (Figure 2), as well as serosa layer composed of abundant collagen fibers and elastic fibers (Figure 1i to l).⁵⁵ These images clearly disclosed the delicate tissue architectures and cellular

features in the 4-layer structure, such as epithelial cells, nuclei, gastric glands, collagen, collagen bundles, elastin, basement membrane, nerves, and blood vessels.⁵⁵ This study reaffirmed that combination of SHG and TPEF signals can accurately identify the histological structures, cellular features, and their boundaries of the gastric wall, and the MPM images matched well with the corresponding hematoxylin-eosin (H&E) images.⁵⁵

MPM Imaging of Precancerous Lesions

MPM has been used in imaging gastric cancer precancerous lesions with a focus on searching for goblet cells whose appearance constitutes a good indicator of IM. Taking mouse intestine as IM model, Bao et al⁵⁶ used 1-photon confocal fluorescence endoscopy (OPFE) and TPFE to perform 3-dimensional imaging of goblet cells. The results showed that both OPFE and TPFE reached a penetration depth of 176 μm in 3-dimensional imaging, and both could image the mucosal surface structure of the mouse intestine, but the slice images of TPFE

Table 1. MPM Imaging of Gastric Cancer at Different T-Stages.⁵⁵

T stage	Characteristic features revealed by MPM imaging
Tis	The epithelial nuclei were abnormally enlarged and the gastric glands were irregular and varied in shape, the borders of the tumor layer were clear, the borders of the lamina propria were well defined, and there were no tumor lesions. TPEF/SHG signals showed intact mucosal, muscularis mucosa, and submucosal layers.
T1	
T1a	Lamina propria was infiltrated by cancer cells with anomalous nuclear sizes, with part of the collagen fibers substituted by tumor cells and muscularis mucosa invaded by tumor cells and lymphoid follicles. The delineation between muscularis mucosa and submucosa was clearly discernible, and no tumor was detected in submucosa.
T1b	The submucosa was thick and dense. TPEF signal showed general infiltration of tumor cells, SHG signal showed the distribution of collagen, and angiogenesis supplying nutrients around cancerous lesions were observed. The delineation between submucosa and muscularis propria was maintained.
T2	The tumor was confined to muscle tissue without serosa infiltration. TPEF signal showed that obvious cancer masses occupied part of muscle tissue and blocked continuous muscle fibers, with most muscle tissues being decomposed. The border between external longitudinal muscle and serosa was present.
T3	The external longitudinal muscle was heavily disrupted. The anomalous gastric gland was composed of cells with enlarged nuclear penetrated muscle tissue and serosa connective tissue, but the serosa margin was intact.
T4	The infiltrating tumor cut off serosa and the margin lost continuity.

Abbreviations: MPM, multiphoton microscopy; TPEF, 2-photon excited fluorescence; SHG, second-harmonic generation.

with different depths showed higher resolution and contrast.⁵⁶ TPEF clearly disclosed the structure of intestinal mucosal filament and goblet cells at 88- μm depth in submucosa, and gland structure even at 176- μm depth in submucosa.⁵⁶ In comparison, TPEF has higher optical sectioning ability but less photobleaching and photodamaging to the intestinal tract of mice.⁵⁶ In another study, Wu et al⁵⁷ identified goblet cells by imaging normal and intestinal gastric tissues using TPEF. They suggested that normal gastric tissues and intestinal gastric tissues can be distinguished by calculating the total number of goblet cells per unit area, that is, the density of goblet cells.

In 2018, Li et al⁴⁹ used spectrum- and time-resolved MPM for the first time to image normal gastric mucosa, chronic gastritis with erosion (CG-E), chronic gastritis with IM (CG-IM) and intestinal-type adenocarcinoma (ITA). As Figure 3 showed, in normal tissue (column A), the superficial epithelium displayed regular cobblestone shape (0- μm depth); both individual mucosal epithelial cells (yellow arrows), and the nuclei (magenta arrows) are clearly visualized.⁴⁹ Slender interstitial tissue containing a small amount of collagen and plasma cells was visible below the surface epithelium and among the gastric pits (orange arrowheads).⁴⁹ The gastric pits showed branching openings in superficial mucosal layer, whereas in their underlying layer they exhibited evenly distributed oval shape and uniform size (white arrowheads).⁴⁹

Compared with normal tissues, diseased specimens had several common features (Columns B, C, D).⁴⁹ For example, the interstitial tissue was significantly wider (orange arrowheads), inflammatory cells increased in number (pink arrows), and the gastric pits became increasingly blurred with disease progression (white arrowheads).⁴⁹ For CG-E specimens (Column B), the mucosal epithelial cells were irregularly spread and uneven in size (yellow arrows), and a few

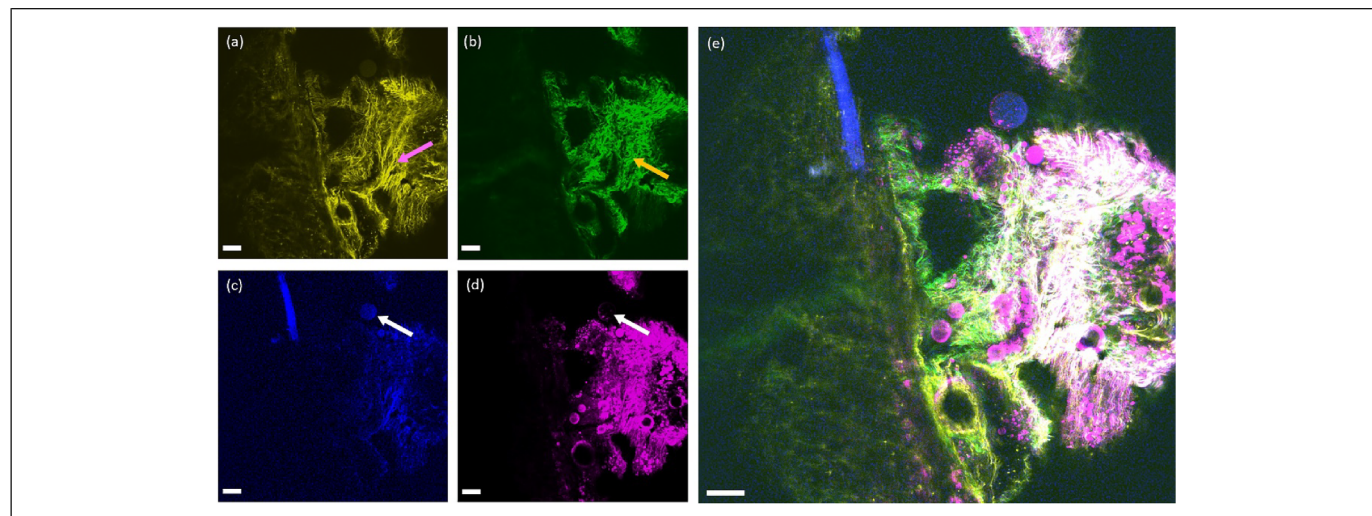


Figure 5. TPEF/SHG/ThPEF/THG images of ex vivo human gastric tissue. (a) TPEF image; (b)SHG image; (c) ThPEF image; (d)THG image; (e)Merging of TPEF/SHG/ThPEF/THG images. pink arrow: elastic fiber; yellow arrow: collagen; white arrow: adipocyte. Scale bar: 100 μm .⁷⁴ Abbreviations: TPEF, 2-photon excited fluorescence; ThPEF, 3-photon excited fluorescence; THG, third-harmonic generation; SHG, second-harmonic generation.

Table 2. Main MPM Studies on Normal or Gastric Cancer Tissues.

References	Imaging modality	Sample type	Pathology/model type	Study	Main findings and criticalities
Rogart et al (2008)	TPEF, SHG	Unfixed, unstained gastrointestinal mucosa		Microscopic examination of intact human gastrointestinal mucosa <i>ex vivo</i>	Improved cellular details relative to confocal imaging.
Bao et al (2009)	TPEF	Mouse intestine	IM model	Imaging of goblet cells as a marker for IM of the stomach	Higher resolution and contrast demonstrated for TPEF compared with confocal endomicroscopy.
Yan et al (2011)	TPEF, SHG	Fresh, unfixed, unstained gastric specimens	Gastric cancer	Pilot study of using multiphoton microscopy to diagnose gastric cancer	Cancerous cellular characteristics such as irregular size and shape, enlarged nuclei, and increased nuclear-to-cytoplasmic ratio.
Chen et al (2011)	TPEF, SHG	Human gastric tissue	Gastric cancer	Establishing diagnostic features for identifying the mucosa and submucosa of normal and cancerous gastric tissues	Mucosal and submucosal microstructures of normal and cancerous gastric tissues, and the distribution and content of abnormal cells in these 2 layers.
Wu et al (2014)	TPEF	Fresh, unfixed, unstained gastric specimens	IM gastric tissues	Label-free identification of IM in the stomach	Significant differences in the population density of goblet cells between normal and IM gastric tissues. Potential demonstrated for MPM to distinguish IM from normal gastric tissue.
Yan et al (2016)	SHG	Fresh, unfixed, and unstained gastric cancer	Gastric cancer with /without serosal invasion	Real-time optical diagnosis of gastric cancer with serosal invasion	Significant differences between gastric cancer without serosal invasion and gastric cancer with serosal invasion; Improved diagnostic accuracy for T4 gastric cancer compared with EUS.
He et al (2018)	TPEF, SHG	Fresh, unfixed, and unstained gastric cancer	Gastric cancer	Label-free imaging for T staging of gastric carcinoma	Gastric normal and tumor tissues under different T stages visually presented with cellular and subcellular features; subcellular and molecular changes during carcinogenesis objectively and quantitatively indicated by TPEF and SHG
Li et al (2018)	TPEF, SHG	Human gastric tissue (gastric antrum)	Chronic gastritis with erosion or IM, intestinal-type adenocarcinoma	Quantitative differentiation of premalignant and malignant gastric mucosa	Qualitative and quantitative indicators with the potential to discriminate the multiple stages of gastric carcinogenesis
Li et al (2019)	TPEF, SHG	Human gastric tissue	Gastric cancer	Label-free monitoring of EGC	Improved cellular detail and stromal changes during the development of EGC
Chen et al (2019)	TPEF, SHG	Unstained serial section human gastric tissue	Gastric cancer	Association of the collagen signature in the tumor microenvironment with lymph node metastasis in EGC	Depth of tumor invasion, tumor differentiation, and the collagen signature were independent predictors of LNM. The prediction model based on this collagen

(continued)

Table 2. (continued)

References	Imaging modality	Sample type	Pathology/model type	Study	Main findings and criticalities
Zheng et al (2020)	TPEF, SHG	Fresh, unfixed gastric cancer	Gastric cancer	Margin diagnosis for endoscopic submucosal dissection of EGC	signature may be useful in treatment decision making for patients with EGC. Cytological and morphological differences accurately identified in the tissue of negative and positive margins of ESD specimens.
Chen et al (2021)	TPEF, SHG	Human gastric tissue	Gastric cancer	Predicting postoperative peritoneal metastasis in gastric cancer with serosal invasion using a collagen nomogram	A competing risk nomogram constructed including collagen characteristics, tumor size, tumor differentiation status, and lymph node metastasis
Wang et al (2022)	TPEF, ThPEF, SHG, THG	Unstained paraffin embedding; Fresh frozen sections		Simultaneous label-free autofluorescence-multiharmonic microscopy imaging	First demonstration of 4 MPM modalities (TPEF, ThPEF, SHG, and THG) on imaging gastric tissues

EGC: early gastric cancer; MPM, multiphoton microscopy; TPEF, 2-photon excited fluorescence; ThPEF, 3-photon excited fluorescence; THG, third-harmonic generation; SHG, second-harmonic generation; EUS, endoscopic ultrasonography; IM, intestinal metaplasia.

mucosal epithelial cells were detached from the epithelium, leading to partial leakage of interstitial tissue to the mucosal surface (orange arrowheads).⁴⁹ In addition, collagen became significantly increased in the interstitial tissue (orange arrowheads).⁴⁹ In the CG-IM lesion tissue (Column C), irregularly located intestinal absorptive cells were visualized in the epithelium (0- μm depth and histological image), goblet cells (red arrows) were found among the absorptive cells, and much less collagen was detected (orange arrowheads).⁴⁹ In the ITA specimens (Column D), regularly spread cancer cells had an absorptive cell-like morphology with a scattering of cancerous goblet cells (0- μm depth, 25- μm depth, and histological image), mitochondrial reduced form of nicotinamide-adenine dinucleotide (NADH) of intestinal absorptive cells (white arrows) displayed a strong fluorescent signal (0- μm depth), and collagen was also barely visible (orange arrowheads).⁴⁹

The results in Figure 3 suggest that the gastric mucosal substructures involving surface epithelium, collagen fibers, and inflammatory cells are well characterized in the MPM images making it possible to differentiate the normal state, different premalignant lesions, and gastric carcinoma.⁴⁹

MPM Imaging of Early and Advanced Cancer

The degree of tumor invasion characterizes the tumor stage, which in turn determines the treatment options and prognosis of gastric cancer. Many research teams have attempted to perform MPM imaging on tumors at different stages in order to provide a basis for clinical treatment selection and prognostic judgment. In 2019, Li et al⁵⁸ examined 12 surgical specimens of EGC and 12 normal gastric tissues using TPEF and SHG imaging, and made a comparison with the histopathological

examination performed on routinely stained specimens. As Figure 4 illustrates, the MPM images clearly display the histological structure and cellular and subcellular structures of EGC with different infiltration depths.⁵⁸ The results discovered epithelial glands abnormally disordered in mucosal tissues with different shapes and disordered extracellular collagen matrix. Elastin fibers in submucosa almost disappeared, and collagen fibers were sparse and broken.⁵⁸ Li et al⁵⁸ also presented quantitative analysis based on measuring the circumference of nucleus and the average intensity of SHG per pixel, which showed that the epithelial cells of EGC exhibited larger size. For example, the nuclear circumference was $47.25 \pm 6.41 \mu\text{m}$ for cancer cells and only $20.32 \pm 2.38 \mu\text{m}$ for normal cells. Meanwhile, collagen grew more compact: the average SHG intensity per pixel was 16.76 ± 1.26 in normal mucosa and 25.59 ± 4.47 in cancerous mucosa. Blind method was used in this study to evaluate the MPM accuracy in detecting EGC. The diagnostic sensitivity, specificity, positive predictive value, and negative predictive value were 91.7%, 100%, 100%, and 92.3%, respectively.

Multiple studies have shown that alterations in collagen in the tumor microenvironment are associated with tumor behavior of cancer and affect cancer invasion and metastasis.^{59–61} In 2019, Chen et al³⁹ carried out a retrospective cohort study that evaluated the risk of lymph node metastasis in patients with gastric cancer who underwent radical gastrectomy for gastric cancer and were confirmed as T1 stage by postoperative pathology. Collagen features were extracted using TPEF and SHG. Multivariate analysis suggested that tumor invasion depth, tumor differentiation degree, and collagen characteristics were independent predictors of lymph node metastasis.³⁹ A prediction model incorporated these 3 predictive factors showed great resolution in the primary cohort (area under the receiver

operating characteristic [AUROC], 0.955; 95% confidence interval [CI], 0.919-0.991) and validation cohort (AUROC, 0.938; 95% CI, 0.897-0.981). In the total of 375 patients, the sensitivity, specificity, accuracy, positive predictive value, and negative predictive value were 87.3%, 92.1%, 91.2%, 72.1%, and 96.9%, respectively.³⁹ This study demonstrated that collagen characteristics in the tumor microenvironment were independent predictors of lymph node metastasis in EGC patients. A predictive model based on the collagen markers may be helpful for treatment decision-making of whether to perform lymph node dissection in EGC patients. In 2021, the same team conducted another similar study to predict the risk of peritoneal metastasis in patients with gastric cancer and serosal infiltration after radical resection.⁴⁰ High-throughput quantitative collagen features were extracted automatically by MPM imaging, and then 4 potential predictors were selected from 146 collagen signatures by LASSO regression. The above collagen features and 3 clinical pathological features (ie, tumor size ≥ 4 cm, tumor differentiation status, and lymph node metastasis) were taken into multivariate analysis.⁴⁰ A competing risk nomogram constructed based on these 4 factors was obviously superior to the clinical pathological prediction model excluding collagen features. The sensitivity, specificity, and accuracy in the overall cohort were 82.0%, 72.4%, and 75.8%, respectively, which provided reliable basis for clinicians to choose appropriate intervention populations.⁴⁰

The Union for International Cancer Control and the American Joint Committee on Cancer TNM [ie, tumor infiltration (T), lymph node metastasis (N) or distant metastasis (M)] staging system of gastric cancer provides an accurate basis for clinical treatment strategy selection, treatment efficacy assessment, and prognosis determination. In 2018, He et al⁵⁵ utilized MPM to observe the unstained sections of fresh gastric tissues of 18 patients undergoing radical gastrectomy, and preliminarily studied the feasibility of T staging of gastric cancer.⁵⁵ These gastric specimens were grouped as 3 Tis, 2 T1a, 3 T1b, 4 T2, 4 T3 and 2 T4. Tumor tissue has obvious structural and cellular atypia compared with normal gastric tissue. The specific manifestations of MPM imaging of gastric cancer tissues in different stages are summarized in Table 1. MPM images are highly consistent with pathological results for gastric cancer of different T stages. Quantitative analysis showed that nuclear areas of cancer cells were about twice larger than that of normal cells ($58.41 \pm 6.06 \mu\text{m}^2$ vs $32.01 \pm 2.89 \mu\text{m}^2$); collagen content (ie, the ratio of SHG pixels to all pixels in each image) was 0.087 ± 0.012 and 0.020 ± 0.007 for normal and cancerous mucosa, respectively ($P < .001$).⁵⁵ The findings of this study indicated that MPM can clearly display the relationship between tumor and normal structure; TPEF and SHG can objectively and quantitatively reflect the changes in subcellular and molecular in the process of cancer without staining intervention.

MPM Imaging in Surgical Treatment

Radical surgery has become the main solution to treat gastric cancer, and different resection methods were developed

depending on the tumor stage. Endoscopic mucosal resection and endoscopic submucosal dissection (ESD) are recommended as alternatives to surgery for EGC.⁶² Active adjuvant and neoadjuvant radiotherapy and chemotherapy have significant survival advantages for advanced tumors with local or distant metastasis.⁶³ Therefore, accurate pretreatment assessment is essential for individualized treatment and prognosis. An MPM imaging study on ESD surgical specimens confirmed⁶⁴ that MPM could accurately distinguish cytological and morphological differences between tissues with positive or negative margin. The sensitivity, specificity, accuracy, negative predictive value, and positive predictive value of MPM in diagnosing the margin of ESD specimen were 97.62%, 75.00%, 94.00%, 95.35%, and 85.71%, respectively.

In 2016, Yan et al⁶⁵ used MPM to image the specimens of 20 patients who underwent radical gastrectomy for gastric cancer, and compared them with H&E staining and Masson's trichrome staining. The results revealed regular collagen structure in gastric cancer without serosa invasion, while irregular collagen structure, collagen loss as well as cell and nuclear polymorphism were found in gastric cancer with serosa invasion.⁶⁵ SHG signal can provide quantitative characteristics and the collagen content of gastric cancer tissues with or without serosa infiltration is 0.36 ± 0.18 versus 0.79 ± 0.16 . In the blind verification, the sensitivity, specificity, and accuracy of endoscopic ultrasonography (EUS) and MPM in the diagnosis of T4 gastric cancer were 70% versus 90%, 66.67% versus 96.67%, and 68.33% versus 93.33%, respectively. Compared with EUS, MPM substantially improved the diagnostic accuracy of T4 gastric cancer.⁶⁵ Real-time in situ imaging of gastric cancer with or without serosal invasion is feasible by using multiphoton laparoscopy, and the implementation of this technique can avoid unnecessary laparotomy.

Multimodal MPM Imaging of Gastric Tissue

MPM relies on an ultrafast laser to serve as the driving source to provide ultra-short optical pulses. Mode-locked Ti:sapphire lasers have become the main workhorse for driving MPM. The ultra-short pulses generated by a Ti:sapphire laser center at about 800 nm and are well-suited to excite SHG and TPEF. This explains why current MPM investigations of gastric tissues were all carried out using these 2 imaging modalities. Apparently, adding more modalities such as THG and ThPEF can provide more information and thus facilitate accurate diagnosis of gastric cancers. Implementation of THG and ThPEF imaging normally demands an ultrafast laser source that emits femtosecond pulses with the center wavelength longer than 1000 nm. Recent years have seen the intensive development of ultrafast laser sources working in the wavelength range of 1000 to 1700 nm to drive multimodal MPM.⁶⁶⁻⁷⁰ In 2018, You et al⁷¹ introduced simultaneous label-free autofluorescence-multiharmonic (SLAM) microscopy: they demonstrated that femtosecond pulses centered at 1110-nm are suitable to simultaneously excite TPEF/ThPEF/SHG/THG signals of cellular and extracellular components in living

tissues. In 2020, Sun et al⁷² conducted *ex vivo* and *in vivo* imaging of fresh human and rat tissues by SLAM and developed a color transforming algorithm to convert SLAM image to the virtually H&E-stained histology-like images. In 2020, Shen et al⁷³ integrated the confocal, SLAM, and fluorescence lifetime microscopy to explore the metastatic and metabolic optical signatures of pancreatic cancers. We recently applied SLAM microscopy to imaging gastric tissues.⁷⁴ We employed fiber-optic self-phase modulation (SPM) to broaden an input narrowband optical spectrum centered at 1030 nm provided by an ultrafast Yb-fiber laser.⁷⁴ The broadened spectrum consists of several isolated spectral lobes, and the peak wavelength of the rightmost spectral lobe can be positioned at 1110 nm by adjusting the input pulse energy. Selection of this rightmost spectral lobe generates 48-fs pulses pulse energy with 15-nJ pulse energy. We used this femtosecond light source to drive MPM imaging of gastric tissue using 4 modalities: TPEF, ThPEF, SHG, and THG.⁷⁴ As Figure 5 shows, imaging of elastic fiber by TPEF and fiber-shaped collagen by SHG can highlight the structure of the surrounding extracellular matrix. Adipocytes can be identified by ThPEF and THG. Such a multimodal MPM driven by 1110-nm pulses based on SPM-enabled spectral selection constitutes an enabling tool to delineate both cellular and extracellular components.⁷⁴ To the best of our knowledge, this work reported the first results on SLAM imaging of gastric tissues.

Discussion and Conclusion

With autofluorescence excitation and harmonic signals, MPM can display tissue structures and characteristic features of the gastrointestinal tract at cellular and subcellular levels. MPM can accurately distinguish normal gastric tissues, precancerous lesions, and tumor tissues, which is of particular importance in evaluating tumor infiltration in mucosa, submucosa, muscular layer, and serosa layer, and assessing residual cancer at the surgical margin. Table 2 summarizes current progress related to gastric cancer research enabled by MPM.

Because it holds promise for many important biomedical applications, MPM has become one of the most active interdisciplinary research areas. Researchers with various backgrounds are continuously pushing MPM technology to improve its imaging capabilities with higher speed, larger penetration depth, better resolution, more modalities, and wider field-of-view.^{69,75–77} Despite the aforementioned advantages, applications of MPM imaging in the study of gastric cancer are still in the early stage compared with other mature imaging technologies based on single-photon excitation, eg, confocal microscopy. Although studies have confirmed that MPM can fit well with the traditional gold standard H&E histopathological diagnosis, more clinical studies are demanded to validate that the occurrence and development of tumors can be evaluated only based on MPM imaging. Current reported results on MPM imaging of gastric tissues were all obtained *ex vivo*; that is, the samples were resected tissues removed from the patients. To make MPM imaging possible for *in vivo*

medical applications including optical biopsy, diagnosis, treatment and tumor monitoring, a crucial and urgent challenge is to develop multiphoton endoscope that is compatible with current gastric endoscopy technology. Indeed, several groups have attempted to miniaturize a bulky multiphoton microscope and implement a multiphoton endoscope, which can enable *in vivo* and *in situ* real-time multimodal imaging.^{56,78–83} In addition to displaying morphological features of normal tissue, precancerous lesions and EGC in terms of tissue structure and cell structure at the cellular and subcellular levels, it may provide information on tissue metabolism and realize functional imaging of tissues. Another crucial question is about the phototoxicity associated with MPM imaging that demands ultrafast laser driving sources. Long-term and systematic studies need to be performed to reveal the dependence of phototoxicity on the imaging parameters (eg, imaging speed, focus, depth etc) and laser parameters (eg, pulse duration and energy, repetition rate, wavelength, average power etc). Ultimately MPM diagnosis of gastric cancers in clinical use should prevent causing any undesired side effects associated with phototoxicity. In practice, introducing MPM to realize “optical biopsy” should minimize the possible disruption for the diagnosis procedure; training pathologists to interpret the MPM images or involving additional imaging specialists working with pathologists are both cumbersome and impractical. In order to facilitate clinical interpretation of MPM images by pathologists, several groups are developing virtual-H&E methods for postprocessing MPM tissue images such that they are color mapped analogously to H&E histopathology.^{72,84,85} Based on MPM imaging, this digital staining approach together with machine learning algorithm can generate virtual transillumination H&E images for pathologists to readily interpret.^{86–88}

In conclusion, MPM has the advantages of nondestructive, larger penetration depth, high resolution, and inherent optical sectioning ability. It does not need the complicated steps of traditional histopathological examination, and thus avoids some drawbacks of biopsy, such as sampling error, cost, risk to patients, and delay in obtaining results. With the rapid advance of ultrafast driving lasers, microscope miniaturization, and machine learning techniques for imaging processing, we believe that more clinical results will emerge in the coming years for MPM applied to the study of gastric cancers.


Declaration of Conflicting Interests


The authors declared no potential conflicts of interest with respect to the research, authorship, and/or publication of this article.


Funding

The author(s) disclosed receipt of the following financial support for the research, authorship, and/or publication of this article: This work was supported by the National Key R&D Program of China, the Strategic Support Force Medical Center Clinical Innovation Topics for Medicine and health of China, Chinese Academy of Sciences, National Natural Science Foundation of China, (grant number Nos. 2021YFB3602602, 19ZX40, YJKYYQ20190034, 62175255).

ORCID iDs

Xiaoying Wang  <https://orcid.org/0000-0002-7228-954X>

Lianyong Li  <https://orcid.org/0000-0002-0852-7005>

Guoqing Chang  <https://orcid.org/0000-0003-3666-5402>

References

- Bray F, Laversanne M, Weiderpass E, Soerjomataram I. The ever-increasing importance of cancer as a leading cause of premature death worldwide. *Cancer Am Cancer Soc.* 2021;127(16):3029-3030.
- Sung H, Ferlay J, Siegel RL, et al. Global cancer statistics 2020: GLOBOCAN estimates of incidence and mortality worldwide for 36 cancers in 185 countries. *CA Cancer J Clin.* 2021;71(3):209-249.
- Xu H, Ji JF, Liang H, Shen L, Zhang XT. Consensus of Chinese expert panel on key difficult points of diagnosis and treatment in gastric cancer (2020 edition). *Chin J Pract Surg.* 2020;40(8):869-904.
- National-Health-Commission-of-the-People'S-Republic-of-China. Specification for diagnosis and treatment of gastric cancer (2018 Edition). *Chin J Digest Med Imageol (Electronic Edition).* 2019;9(3):118-144.
- Fock KM, Talley N, Moayyedi P, et al. Asia-Pacific consensus guidelines on gastric cancer prevention. *J Gastroen Hepatol.* 2008;23(3):351-365.
- Ikoma N, Blum M, Chiang YJ, et al. Survival rates in T1 and T2 gastric cancer: a Western report. *J Surg Oncol.* 2016;114(5):602-606.
- Suzuki H, Oda I, Abe S, et al. High rate of 5-year survival among patients with early gastric cancer undergoing curative endoscopic submucosal dissection. *Gastric Cancer.* 2016;19(1):198-205.
- Kim HH, Han SU, Kim MC, et al. Effect of laparoscopic distal gastrectomy vs open distal gastrectomy on long-term survival among patients with stage I gastric cancer: The KCLASS-01 randomized clinical trial. *Jama Oncol.* 2019;5(4):506-513.
- Barad Y, Eisenberg H, Horowitz M, Silberberg Y. Nonlinear scanning laser microscopy by third harmonic generation. *Appl Phys Lett.* 1997;70(8):922-924.
- Denk W, Strickler JH, Webb WW. Two-photon laser scanning fluorescence microscopy. *Science.* 1990;248(4951):73-76.
- Franken PA, Hill AE, Peters CW, Weinreich G. Generation of optical harmonics. *Phys Rev Lett.* 1961;7(4):118-119.
- Göppert-Mayer M. Über Elementarakte mit zwei Quantensprüngen. *Ann Phys-Berlin.* 1931;401(3):273-294.
- König K. Multiphoton microscopy in life sciences. *J Microsc.* 2000;200(Pt 2):83-104.
- Zipfel WR, Williams RM, Webb WW. Nonlinear magic: multiphoton microscopy in the biosciences. *Nat Biotechnol.* 2003;21(11):1369-1377.
- Campagnola P. Second harmonic generation imaging microscopy: applications to diseases diagnostics. *Anal Chem.* 2011;83(9):3224-3231.
- Yelin D, Silberberg Y. Laser scanning third-harmonic-generation microscopy in biology. *Opt Express.* 1999;5(8):169-175.
- Débarre D, Supatto W, Pena AM, et al. Imaging lipid bodies in cells and tissues using third-harmonic generation microscopy. *Nat Methods.* 2006;3(1):47-53.
- Parodi V, Jacchetti E, Osellame R, et al. Nonlinear optical microscopy: From fundamentals to applications in live bioimaging. *Front Bioeng Biotechnol.* 2020;8:585363.
- Hortholary T, Carrion C, Chouzenoux E, Pesquet JC, Lefort C. Multiplex-multiphoton microscopy and computational strategy for biomedical imaging. *Microsc Res Tech.* 2021;84(7):1553-1562.
- Cho HJ, Chun HJ, Kim ES, Cho BR. Multiphoton microscopy: an introduction to gastroenterologists. *World J Gastroenterol.* 2011;17(40):4456-4460.
- Matsui T, Mizuno H, Sudo T, et al. Non-labeling multiphoton excitation microscopy as a novel diagnostic tool for discriminating normal tissue and colorectal cancer lesions. *Sci Rep.* 2017;7(1):6959.
- Rogart JN, Nagata J, Loeser CS, et al. Multiphoton imaging can be used for microscopic examination of intact human gastrointestinal mucosa ex vivo. *Clin Gastroenterol Hepatol.* 2008;6(1):95-101.
- Williams RM, Zipfel WR, Webb WW. Multiphoton microscopy in biological research. *Curr Opin Chem Biol.* 2001;5(5):603-608.
- Rubart M. Two-Photon microscopy of cells and tissue. *Circ Res.* 2005;95(12):1154-1166.
- Lefort C, Chalvidal M, Parente A, et al. FAMOUS: a fast instrumental and computational pipeline for multiphoton microscopy applied to 3D imaging of muscle ultrastructure. *J Phys D: Appl Phys.* 2021;54(27):274005.
- Ramos-Gomes F, Bode J, Sukhanova A, et al. Single- and two-photon imaging of human micrometastases and disseminated tumour cells with conjugates of nanobodies and quantum dots. *Sci Rep.* 2018;8(1):4595.
- Maestro LM, Ramírez-Hernández JE, Bogdan N, et al. Deep tissue bio-imaging using two-photon excited CdTe fluorescent quantum dots working within the biological window. *Nanoscale.* 2012;4(1):298-302.
- Müller M, Squier J, Wilson KR, Brakenhoff GJ. 3D Microscopy of transparent objects using third-harmonic generation. *J Microsc.* 1998;191(3):266-274.
- Boissonnas A, Scholer-Dahire A, Fetler L, Amigorena S. Multiphoton imaging of cytotoxic T lymphocyte-mediated antitumor immune responses. *Curr Top Microbiol Immunol.* 2009;334:265-287.
- Brown EB, Campbell RB, Tsuzuki Y, et al. In vivo measurement of gene expression, angiogenesis and physiological function in tumors using multiphoton laser scanning microscopy. *Nat Med.* 2001;7(7):864-868.
- Horton NG, Wang K, Kobat D, et al. In vivo three-photon microscopy of subcortical structures within an intact mouse brain. *Nat Photonics.* 2013;7(3):205-209.
- Le T, Rehner CW, Huff TB, et al. Nonlinear optical imaging to evaluate the impact of obesity on mammary gland and tumor stroma. *Mol Imaging.* 2007;6(3):205-211.
- Mohler W, White J. Multiphoton laser scanning microscopy for four-dimensional analysis of caenorhabditis elegans embryonic development. *Opt Express.* 1998;3(9):325-331.

34. Ouzounov DG, Horton N, Wang T, Feng D, Xu C. In Vivo Three-photon Calcium Imaging of Brain Activity from Layer 6 Neurons in Mouse Brain. 2014.
35. Paoli J, Smedh M, Wennberg AM, Ericson MB. Multiphoton laser scanning microscopy on non-melanoma skin cancer: morphologic features for future non-invasive diagnostics. *J Invest Dermatol.* 2008;128(5):1248-1255.
36. Sidani M, Wyckoff J, Xue C, Segall JE, Condeelis J. Probing the microenvironment of mammary tumors using multiphoton microscopy. *J Mammary Gland Biol Neoplasia.* 2006;11(2):151-163.
37. Supatto W, Truong TV, Débarre D, Beaurepaire E. Advances in multiphoton microscopy for imaging embryos. *Curr Opin Genet Dev.* 2011;21(5):538-548.
38. Wyckoff J, Gligorijevic B, Entenberg D, Segall J, Condeelis J. High-resolution multiphoton imaging of tumors in vivo. *Cold Spring Harb Protoc.* 2011;2011(10):1167-1184.
39. Chen D, Chen G, Jiang W, et al. Association of the collagen signature in the tumor microenvironment with lymph node metastasis in early gastric cancer. *JAMA Surg.* 2019;154(3):e185249.
40. Chen D, Liu Z, Liu W, et al. Predicting postoperative peritoneal metastasis in gastric cancer with serosal invasion using a collagen nomogram. *Nat Commun.* 2021;12(1):179.
41. Karimian-Jazi K, Münch P, Alexander A, et al. Monitoring innate immune cell dynamics in the glioma microenvironment by magnetic resonance imaging and multiphoton microscopy (MR-MPM). *Theranostics.* 2020;10(4):1873-1883.
42. Li L, Han Z, Qiu L, et al. Evaluation of breast carcinoma regression after preoperative chemotherapy by label-free multiphoton imaging and image analysis. *J Biophotonics.* 2020;13(1):e201900216.
43. Provenzano PP, Eliceiri KW, Keely PJ. Multiphoton microscopy and fluorescence lifetime imaging microscopy (FLIM) to monitor metastasis and the tumor microenvironment. *Clin Exp Metastasis.* 2009;26(4):357-370.
44. Qiu J, Jiang W, Yang Y, et al. Monitoring changes of tumor microenvironment in colorectal submucosa using multiphoton microscopy. *Scanning.* 2015;37(1):17-22.
45. Barhoumi R, Catania JM, Parrish AR, et al. Multiphoton spectral analysis of benzo[a]pyrene uptake and metabolism in breast epithelial cell lines. *J Toxicol Sci.* 2009;34(1):13-25.
46. Fang N, Wu Z, Wang X, et al. Quantitative assessment of microenvironment characteristics and metabolic activity in glioma via multiphoton microscopy. *J Biophotonics.* 2019;12(10):e201900136.
47. Feinauer MJ, Schneider SW, Berghoff AS, et al. Local blood coagulation drives cancer cell arrest and brain metastasis in a mouse model. *Blood.* 2021;137(9):1219-1232.
48. Li LH, Chen ZF, Wang XF, et al. Multiphoton microscopy for tumor regression grading after neoadjuvant treatment for colorectal carcinoma. *World J Gastroenterol.* 2015;21(14):4210-4215.
49. Li X, Li H, He X, et al. Spectrum- and time-resolved endogenous multiphoton signals reveal quantitative differentiation of premalignant and malignant gastric mucosa. *Biomed Opt Express.* 2018;9(2):453-471.
50. Zhuo S, Chen J, Wu G, et al. Label-free multiphoton imaging and photoablation of preinvasive cancer cells. *Appl Phys Lett.* 2012;100(2):023703.
51. Correa P, Houghton J. Carcinogenesis of Helicobacter pylori. *Gastroenterology.* 2007;133(2):659-672.
52. Chen J, Zhuo S, Chen G, et al. Establishing diagnostic features for identifying the mucosa and submucosa of normal and cancerous gastric tissues by multiphoton microscopy. *Gastrointest Endosc.* 2011;73(4):802-807.
53. Kumar V, Abbas AK, Aster JC. Robbins Basic Pathology, Tenth Edition. 2018.
54. Yan J, Chen G, Chen J, et al. A pilot study of using multiphoton microscopy to diagnose gastric cancer. *Surg Endosc.* 2011;25(5):1425-1430.
55. He K, Zhao L, Huang X, et al. Label-free imaging for T staging of gastric carcinoma by multiphoton microscopy. *Lasers Med Sci.* 2018;33(4):871-882.
56. Bao H, Boussioutas A, Reynolds J, Russell S, Gu M. Imaging of goblet cells as a marker for intestinal metaplasia of the stomach by one-photon and two-photon fluorescence endomicroscopy. *J Biomed Opt.* 2009;14(6):064031.
57. Wu G, Wei J, Zheng Z, Ye J, Zeng S. Label-free identification of intestinal metaplasia in the stomach using multiphoton microscopy. *Laser Phys Lett.* 2014;11(11):065602.
58. Li L, Kang D, Huang Z, et al. Multimodal multiphoton imaging for label-free monitoring of early gastric cancer. *BMC Cancer.* 2019;19(1):295.
59. Conklin MW, Gangnon RE, Sprague BL, et al. Collagen alignment as a predictor of recurrence after ductal carcinoma in situ. *Cancer Epidemiol Biomarkers Prev.* 2018;27(2):138-145.
60. Pointer KB, Clark PA, Schroeder AB, et al. Association of collagen architecture with glioblastoma patient survival. *J Neurosurg.* 2017;126(6):1812-1821.
61. Provenzano PP, Inman DR, Eliceiri KW, et al. Collagen density promotes mammary tumor initiation and progression. *BMC Med.* 2008;6(1):1-15.
62. Pimentel-Nunes P, Dinis-Ribeiro M, Ponchon T, et al. Endoscopic submucosal dissection: European society of gastrointestinal endoscopy (ESGE) guideline. *Endoscopy.* 2015;47(9):829-854.
63. Roukos DH. Current status and future perspectives in gastric cancer management. *Cancer Treat Rev.* 2000;26(4):243-255.
64. Zheng X, Zuo N, Lin H, et al. Margin diagnosis for endoscopic submucosal dissection of early gastric cancer using multiphoton microscopy. *Surg Endosc.* 2020;34(1):408-416.
65. Yan J, Zheng Y, Zheng X, et al. Real-time optical diagnosis of gastric cancer with serosal invasion using multiphoton imaging. *Sci Rep.* 2016;6(1):1-8.
66. Hsiang-Yu C, Wei L, Qian C, et al. Tunable, ultrafast fiber-Laser between 1.15 and 1.35 μm for harmonic generation microscopy in human skin. *Ieee J Sel Top Quant.* 2018;25(1):1-8.
67. Liao YH, Su YH, Shih YT, et al. In vivo third-harmonic generation microscopy study on vitiligo patients. *J Biomed Opt.* 2019;25(1):1-13.
68. Liu W, Chia SH, Chung HY, et al. Energetic ultrafast fiber laser sources tunable in 1030-1215 nm for deep tissue multi-photon microscopy. *Opt Express.* 2017;25(6):6822-6831.
69. Wang T, Xu C. Three-photon Neuronal Imaging in Deep Mouse Brain. *Optica.* 2020;7(8):947-960.

70. Zhang H, Chen Y, Cao D, et al. Optical biopsy of laryngeal lesions using femtosecond multiphoton microscopy. *Biomed Opt Express*. 2021;12(3):1308-1319.
71. You S, Tu H, Chaney EJ, et al. Intravital imaging by simultaneous label-free autofluorescence-multiharmonic microscopy. *Nat Commun*. 2018;9(1):2125.
72. Sun Y, You S, Du X, et al. Real-time three-dimensional histology-like imaging by label-free nonlinear optical microscopy. *Quant Imaging Med Surg*. 2020;10(11):2177-2190.
73. Shen B, Yan J, Wang S, et al. Label-free whole-colony imaging and metabolic analysis of metastatic pancreatic cancer by an autoreregulating flexible optical system. *Theranostics*. 2020;10(4):1849-1860.
74. Wang X, Xing Y, Chen R, et al. Label-free autofluorescence multifrequency microscopy system based on self-phase modulation enabled spectral selection source. *Acta Phys Sin-Ch Ed*. 2022;71(10):224-231.
75. Lecoq J, Orlova N, Grewe BF. Wide. Fast. Deep: Recent advances in multiphoton microscopy of in vivo neuronal activity. *J Neurosci*. 2019;39(46):9042-9052.
76. Papagiakoumou E, Ronzitti E, Emiliani V. Scanless two-photon excitation with temporal focusing. *Nat Methods*. 2020;17(6):571-581.
77. Wu J, Ji N, Tsia KK. Speed scaling in multiphoton fluorescence microscopy. *Nat Photonics*. 2021;15(11):800-812.
78. Chen X, Xu X, McCormick DT, Wong K, Wong ST. Multimodal nonlinear endo-microscopy probe design for high resolution, label-free intraoperative imaging. *Biomed Opt Express*. 2015;6(7):2283-2293.
79. Dilipkumar A, Al-Shemmary A, Kreiß L, et al. Label-Free multiphoton endomicroscopy for minimally invasive in vivo imaging. *Adv Sci (Weinh)*. 2019;6(8):1801735.
80. Hwang K, Seo YH, Jeong KH. Microscanners for optical endomicroscopic applications. *Micro Nano Syst Lett*. 2017;5(1):1-11.
81. Kudlinski A, Cassez A, Vanvincq O, et al. Double clad tubular anti-resonant hollow core fiber for nonlinear microendoscopy. *Opt Express*. 2020;28(10):15062-15070.
82. Lukic A, Dochow S, Bae H, Matz G, Popp J. Endoscopic fiber probe for nonlinear spectroscopic imaging. *Optica*. 2017;4(5):496.
83. Pshenay-Severin E, Bae H, Reichwald K, et al. Multimodal nonlinear endomicroscopic imaging probe using a double-core double-clad fiber and focus-combining micro-optical concept. *Light Sci Appl*. 2021;10(1):207.
84. Tao YK, Shen D, Sheikine Y, et al. Assessment of breast pathologies using nonlinear microscopy. *Proc Natl Acad Sci U S A*. 2014;111(43):15304-9.
85. Giacomelli MG, Husvogt L, Vardeh H, et al. Virtual hematoxylin and eosin transillumination microscopy using epi-fluorescence imaging. *Plos One*. 2016;11(8):e0159337.
86. Borhani N, Bower AJ, Boppart SA, Psaltis D. Digital staining through the application of deep neural networks to multi-modal multi-photon microscopy. *Biomed Opt Express*. 2019;10(3):1339-1350.
87. de Haan K, Zhang Y, Zuckerman JE, et al. Deep learning-based transformation of H&E stained tissues into special stains. *Nat Commun*. 2021;12(1):4884.
88. Rivenson Y, Haan KD, Wallace WD, Ozcan A. Emerging advances to transform histopathology using virtual staining. *BME Front*. 2020;1(1):11.